Chapter 4

Layered double hydroxides-polymer nanoconjugate for the enhancement of cellular uptake and controlled delivery of hydrophobic anticancer drug

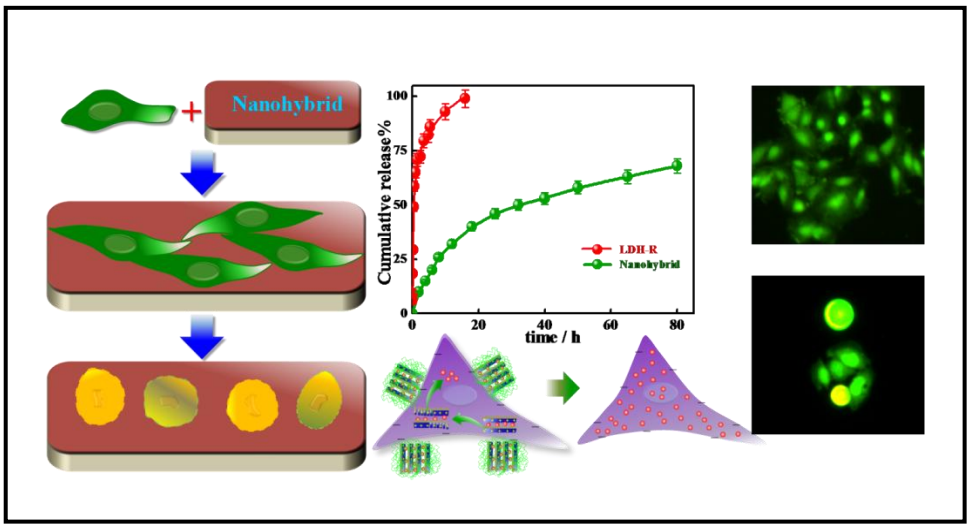

A model anti cancer drug has been intercalated within two-dimensional Zn-Fe based LDHs to have sand witched structure followed by its embedment in polymer matrix for designing novel drug delivery vehicle with sustained release, greater bioavailability and advanced anti-tumor efficacy without any adverse effect as opposed to conventional chemotherapeutic treatment of cancer.

4.1 Introduction

Although conventional chemotherapy is effective to some extent, chemotherapeutic drug induces severe unintended and undesirable side effects such as major organ damage, immunosuppression, loss of appetite, infertility and nausea / vomiting. The chemotherapy drugs often suffer from critical obstacles like poor solubility, poor cellular uptake, drug instability and have severe adverse effects on normal organs. In order to enhance therapeutic efficacy, reduce toxicity and frequency of drug administration, a numerous numbers of drug delivery systems have been developed over past few decades. Among them nanotechnology is getting considerable attention in recent years to bring new hope for chemotherapy [Thakor et al., 2013; Khandelia et al., 2013; Zelasko-Leon et al., 2015]. Layered double hydroxide nanoparticles are considered as one of the potent nanocarrier due to their excellent anion exchange capacity, excellent biocompatibility, high loading capacity, full protection for the loaded therapeutic agents, facile preparation methods, biodegraded in the cellular cytoplasm (pH = 4–6), pH dependent stability, low cost and release, and excellent endosome escape. LDHs structure consist of cationic brucite-like layers and exchangeable anionic species in the interlayer galleries and posses excellent anion exchange capability negatively charged drugs, DNA molecules, peptides or any bioactive molecules. Hence, LDHs has the capability for efficient intracellular delivery of such membrane-impermeable therapeutic agents since it markedly reduces the electrostatic repulsive interactions between the negatively charged cell membrane and anionic bioactive agents [Choy et al., 2000; Xu et al., 2006; Choi et al., 2011]. However, these LDHs based systems have very fast *in vitro* release profile, release almost 100% drugs within couple of hours [Khan et al., 2002; Djebbi et al., 2016]. Again, LDH-drug nanohybrids also have very fast *in vivo* release properties [Choi et al., 2010]. Again, the net surface positive charge of LDHs can interact with negatively charged plasma proteins and influences their pharmacokinetic properties and shortens their blood residence time.

Biodegradable, biocompatible polymers are considered as attractive materials to deliver the drug in a sustained manner. Amongst them, FDA approved poly(ε-caprolactone) (PCL) is known as one of the efficient biomaterials for its facile biodegradation nature, enzymatic cleavage at physiological conditions generating non-toxic by-products, biocompatibility, good mechanical properties, chemical and thermal stability and tissue-compatible nature used for wide range of applications such as implantable devices and has the potential of acting as a controlled drug delivery carrier [Woodruff et al., 2010; Rai et al., 2016]. However, PCL is hydrophobic in nature, causing weak cell-material interactions and thus has poor cell adhesion behaviors [Goddard et al., 2007; Zhu et al., 2002]. The weaker the cell-material interaction (cell adhesion), lower will be the cellular uptake efficacy. It is therefore expected that the development of nanohybrid will provide advantages of LDH nanoparticle and polymer vector while overcoming their shortcomings.

The present chapter deals with the development of a novel nanohybrid drug delivery carrier by embedding drug intercalated layered double hydroxide in PCL matrix to enhance the therapeutic efficacy of the hydrophobic anticancer drugs by improving bioavailability, *in vitro* and *in vivo* prolonged and sustained drug release characteristics, superior cellular uptake, improved cancer cell killing efficiency while reducing *in vivo* adverse effects to other body tissues by proper balancing the hydrophilic–hydrophobic ratio. Various *in vitro* and *in-vivo* experiments have been performed to investigate the efficacy of this novel drug vehicle.

4.2 Results and Discussion

4.2.1 Synthesis of various Zn-Fe based layered double hydroxide nanoparticles

Three different layered double hydroxides have been synthesized by using coprecipitaion technique from the zinc and iron salts with varying charge density interlayer anions such

as nitrate (NO_3^{-1}), carbonate (CO_3^{-2}), phosphate (PO_4^{-3}) and are abbreviated as ZN, ZC and ZP respectively. Elemental constitution and the presence of the anions are confirmed by using Energy Dispersive X-ray Spectrometry (EDS) exhibiting characteristic peak of Fe and Zn in addition to the detailed composition of all three LDHs, ZN, ZC and ZP, (**Figure 4.1**).

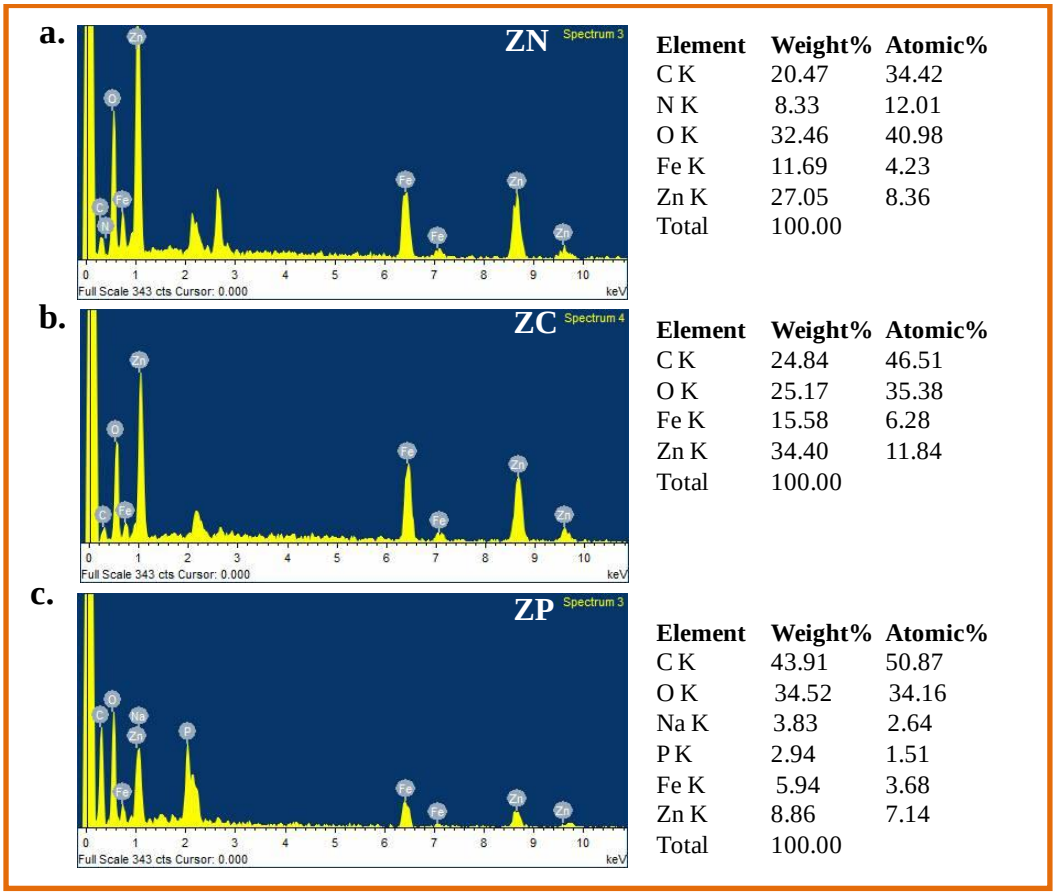

Element	Weight%	Atomic%
C K	20.47	34.42
N K	8.33	12.01
O K	32.46	40.98
Fe K	11.69	4.23
Zn K	27.05	8.36
Total	100.00	

Element	Weight%	Atomic%
C K	24.84	46.51
O K	25.17	35.38
Fe K	15.58	6.28
Zn K	34.40	11.84
Total	100.00	

Element	Weight%	Atomic%
C K	43.91	50.87
O K	34.52	34.16
Na K	3.83	2.64
P K	2.94	1.51
Fe K	5.94	3.68
Zn K	8.86	7.14
Total	100.00	

Figure 4.1: Energy dispersive X-ray spectrum of ZN, ZC and ZP LDH nanoparticles.

The bright field TEM images all the three LDHs particles exhibit circular platelet-like shape with lateral dimension of ~80 nm with moderate distribution of particle size (**Figure 4.2a**). Again, selected area electron diffraction (SAED) patterns of ZN, ZC and ZP nanoparticles reveal the presence of concentric diffraction rings with characteristics of Zn based LDH; (018), (110) and (113) planes confirming the crystalline natures of the LDH nanoparticles (**Figure 4.2b**) [Carja et al., 2010; Mohapatra et al., 2014]. The disc

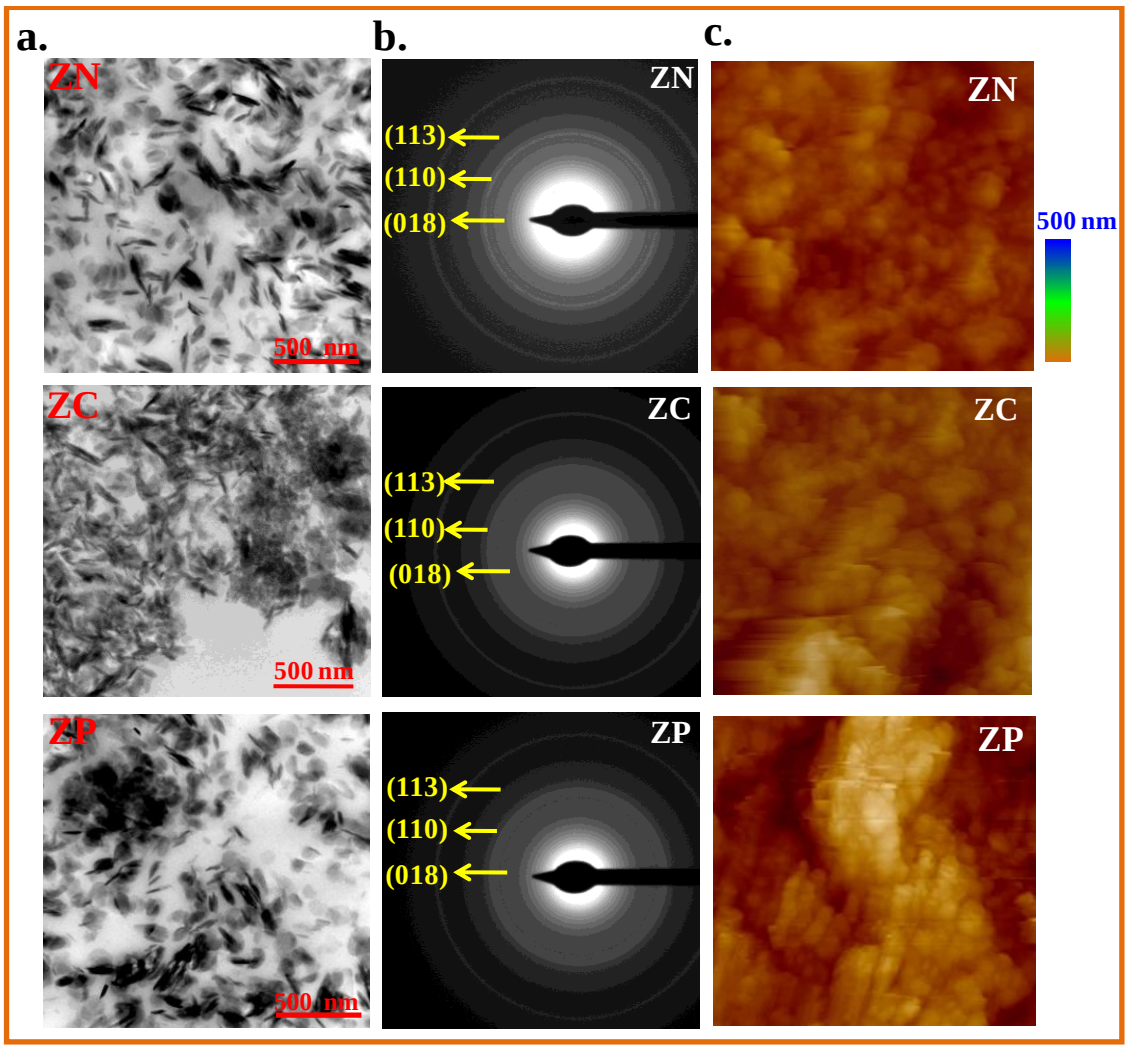

Figure 4.2: (a) High-resolution transmission electron microscopic image of platelet like shape of ZN, ZC and ZP LDH nanoparticles. (b) SAED patterns of ZN, ZC and ZP LDHs showing various planes of LDHs; (c) AFM topographical images of the samples after spin-coated on a SiO_2/Si glass substrate.

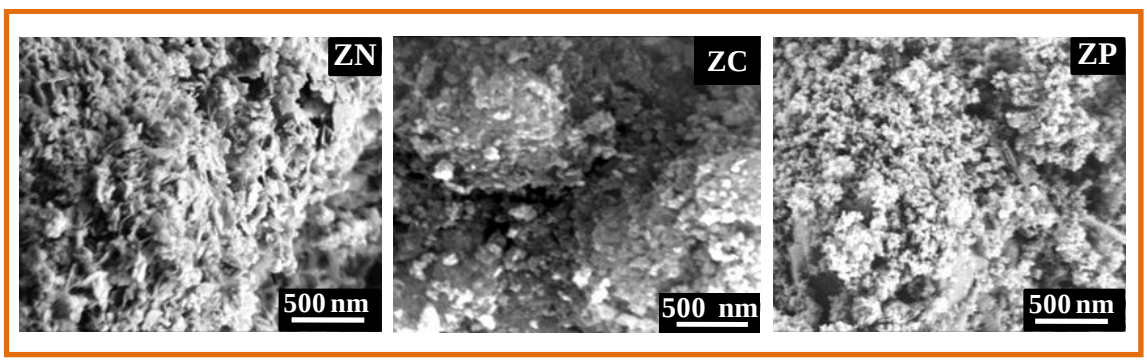

Figure 4.3: SEM images of pristine ZN, ZC and ZP LDH nanoparticles.

like morphology of the LDH nanoparticles is also confirmed by using AFM images (**Figure 4.2c**) with average particle diameter of ~85 nm. In SEM analysis, ZN shows flake-like morphology, whereas ZC and ZP exhibit granular morphology (**Figure 4.3**).

4.2.2 Intercalation of drug within LDH interlayer and its embedment in polymer

Hydrophobic anti-tumor drug (raloxifene) has been intercalated into LDH interlayer galleries through ion exchange technique by replacing the NO_3^{-1}, CO_3^{-2} and PO_4^{-3} anions from the respective LDHs. The intercalation of drug is confirmed from the appearance of a new XRD peak at $2\theta \sim 6.7^o$ in ZN-R (indicated with the '∗' mark), resulting to an increase in the interlayer height of 1.32 nm from the strong peak of pure ZN at $2\theta \sim 11.34^o$ (d ~ 0.834 nm) associated with (003) basal plane of pristine LDH (**Figure 4.4a**). However, the intercalated peak becomes less intense in PN-R (polymer nanoconjugate) due to disordered structure of ZN-R in polymer matrix. The higher order diffraction peaks arising from (006) and (009) basal planes, along with other basal planes of (110) and (113) suggest the crystallized hydrotalcite-like structure with a rhombohedral like packing of the 2-D LDHs molecules [Evans et al., 2006; Gago et al., 2008]. However, these crystalline peaks become weaker and broader in ZN-R and PN-R (nanohybrid) due to incorporation of drug molecules into the interlayer gallery of ZN-R and its dispersed phase structure in PCL matrix as compared to pristine ZN. Pure PCL exhibits sharp crystalline peaks at 2θ 21.5^o and 23.85^o assigned to the (110) and (200) basal planes which is slightly shifted after the embedment of ZN-R in polymer matrix due to interaction. Furthermore, the effect of drug intercalation has a marked influence on the morphology of ZN-R where the stacking of platelets is clearly observed with lateral dimension of 90±7 nm (**Figure 4.4b**) due to agglomeration. The SAED pattern of ZN–R particle shows the presence of concentric diffraction rings (inset of **Figure 4.4b**) against a corona around the pointer in PN-R nanoconjugate, indicating the existence of large

poly-crystalline structure of LDH in polymer matrix. On the other hand, dispersed morphology of ZN-R is evident in PN-R. Discrete particle morphology is observed in AFM measurement with periodic height profile of ZN-R while smooth surface morphology in pristine PCL which subsequently

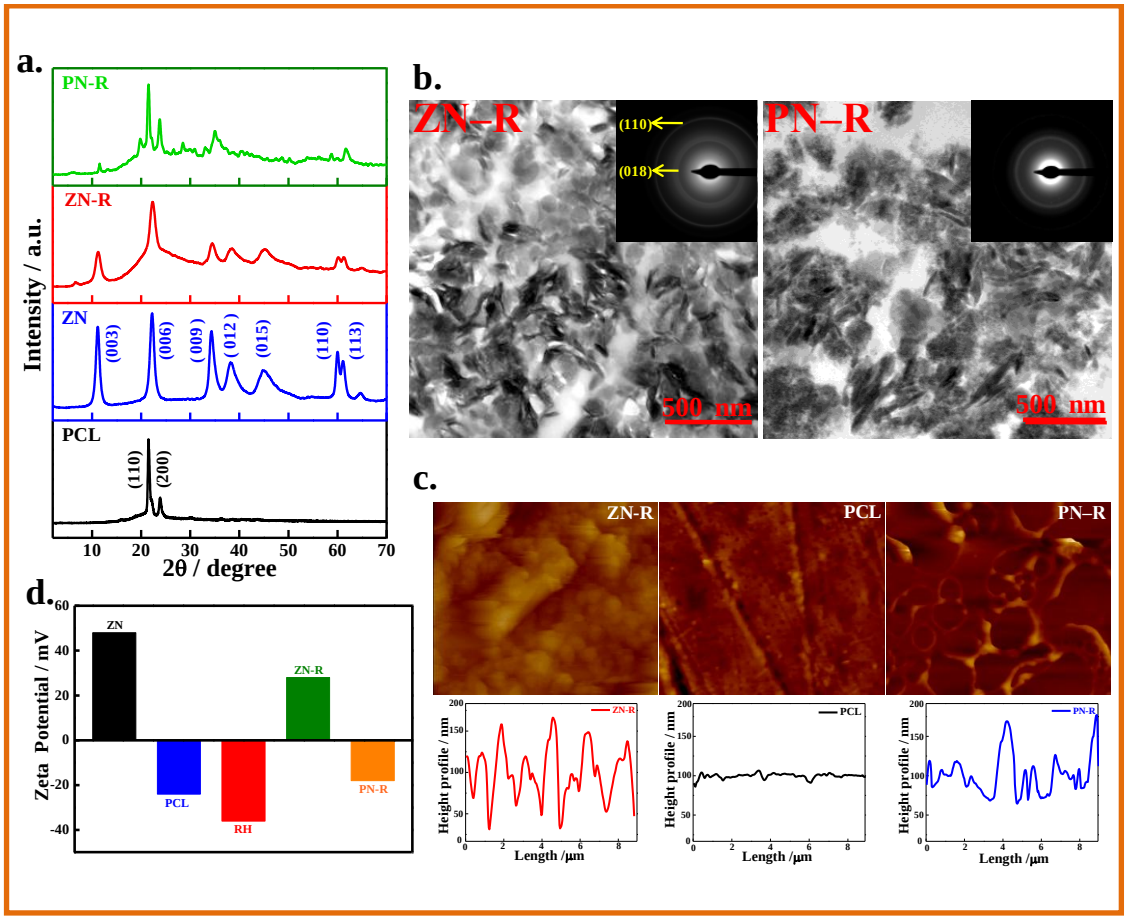

Figure 4.4: (a) Powder X-ray diffraction patterns of pristine PCL, pristine ZN, ZN–R and PN–R, '⋆' marks indicate the new set of basal reflections which originates from RH intercalated LDH phases; (b) TEM images of ZN–R and PN–R samples, inset shows the SAED patterns of ZN–R and PN–R; (c) Zeta potentials of the developed samples; and (d) AFM topographs of ZN–R, PCL and PN–R with corresponding height profiles exhibiting relative surface roughness.

periodic again in PN-R (nanohybrid) showing the marked influence of drug embedded nanoparticle in polymer matrix (**Figure 4.4c**). Surface charge, a key parameter for biologically active molecule to pass across the cell membrane, has been measured by

using zeta potential and high positive and negative values of 48±5 and −33±4 mV are detected for ZN (pristine LDH) and RH (pure drug), respectively, and drug intercalation in LDH reduce its zeta potential to 27±3 mV. Moreover, the zeta potential of ZN-R embedded nanoconjugate exhibits a moderate value of −18±2 mV in PN-R considering the zeta potential of pristine PCL of −22±2 mV (**Fig. 4.4d**). Thus, surface charge of the pure drug has been regulated by intercalating the drug into LDH layers and subsequently embedding it into the polymer matrix for improved drug bioavailability and sustained release of the drug in biological media.

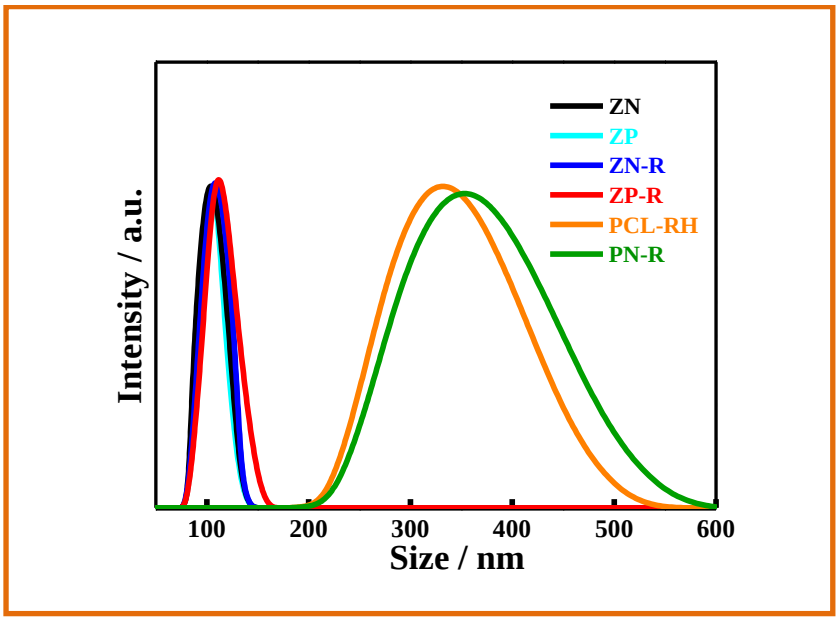

Figure 4.5 DLS particle size distribution of ZN, ZN-R, PCL-RH and PN-R which were found to be 100±4, 110±3, 315±4 and 332±3 nm with polydispersity index (PDI) of 0.19, 0.22, 0.17 and 0.20 respectively.

The size distribution of LDH particles before and after drug intercalation has also been measured by using dynamic light scattering (DLS) technique of ZN, ZN-R, PCL-RH and PN-R which were found to be 100±4, 110±3, 315±4 and 332±3 nm respectively **Figure 4.5**.

4.2.3 *In vitro* controlled release of drug

Controlled release of drug is crucial especially for cancer treatment to maintain the drug concentration level within the therapeutic window for a desired period of time to avoid disastrous side effect of the drug. *In vitro* release characteristics of raloxifene from the three different drug intercalated LDHs, PCL matrix and PCL nanoconjugate has been studied through UV-Vis absorption spectroscopy. **Figure 4.6a** demonstrates the cumulative percentage release of raloxifene in PBS media (pH ~ 7.4) at 37 ^{o}C. ZP–R (phosphate ion as intercalant in LDH) follows burst release profile, about 50% of the drug is released in just 15 min and almost 100% release occurs within 5 h. Though initial burst release is noticed for ZN-R (nitrate ion as intercalant in LDH) system while it follows a slow release kinetics pursuing a biphasic elution profile and continues to release for 36 h. Hence, a gradual sustained drug release rate from ZP-R to ZC-R to ZN-R with varying charge density of intercalant from 3 (phosphate) to 1 (nitrate) primarily due to greater interaction between drug and LDHs. When the drug is embedded directly in PCL matrix (PCL–RH), it exhibits a steady release while unique sustained release of drug is obtained only from PN-R nanoconjugate where drug intercalated LDH is embedded in the polymer matrix. Interestingly, the initial drug release rate is considerably high (35% in 24 h), as per the requirement of therapeutics, followed by a more sustained release kinetics (60% in 80 h). However, steady and sustained release behaviour is observed from PN-R (polymer nanohybrid) for prolonged period of time. For drug intercalated LDHs, drug molecules released from these nanohybrids through anion-exchange of the drug anions by phosphate ions present in PBS medium. In contrast, for PN-R nanoconjugate the entrapped drug molecules are released from the intercalated LDH to polymer matrix first followed by its release to actual media through diffusion process. The schematics of this typical drug release mechanism has been

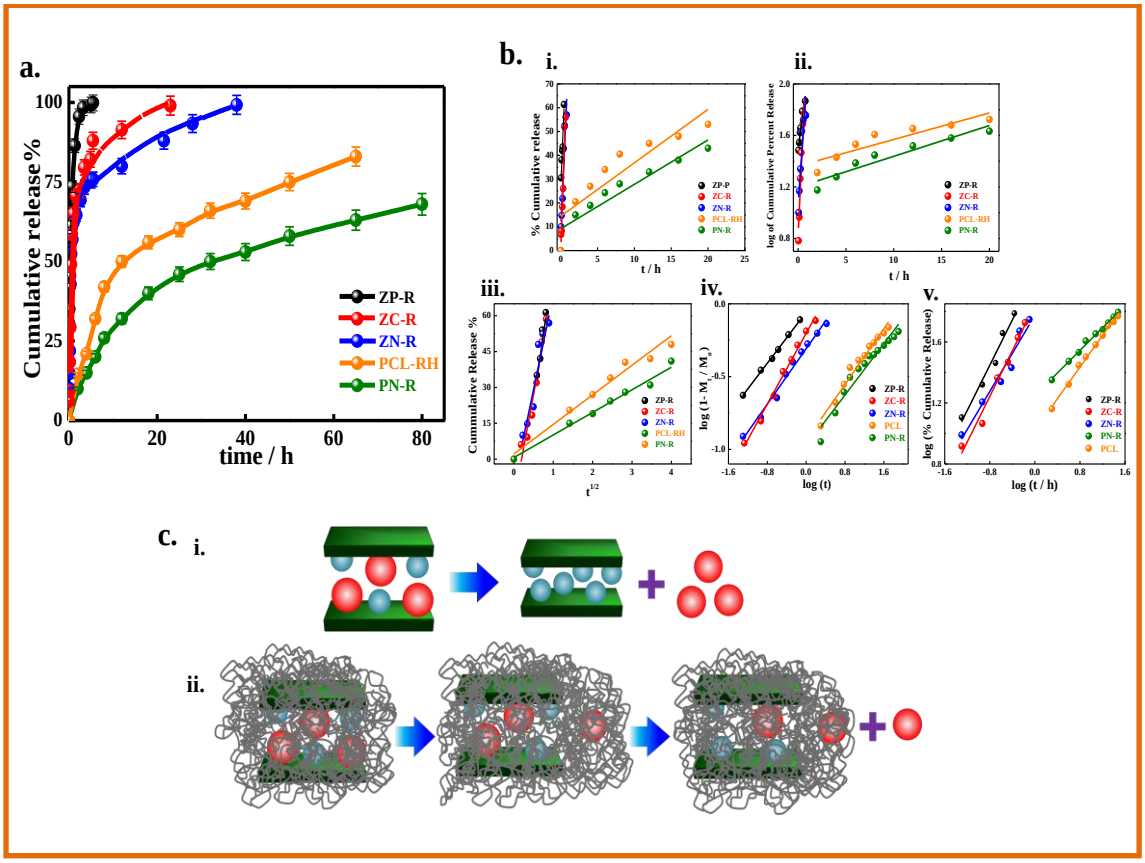

Figure 4.6: (a) Cumulative drug release profile for raloxifene intercalated LDH systems (ZN-R, ZC-R and ZP-R), raloxifene embedded in PCL (PCL-RH) and PCL coated ZN-R (PN-R) in PBS at pH ~7.4 at 37 °C. The results are plotted as mean ± SD values obtained from three different set of experiments; (b) Linear fitting of the drug release data to (i) Zero-order, (ii) first-order, (iii) Higuchi, (iv) modified-Freundlich modified, and (v) Korsmeyer–Peppas model; and (c) Schematic representation of possible drug release mechanisms; (i) in drug intercalated LDHs, (ii) in PN-R.

presented in **Figure 4.6b** showing first release for ZN-R nanohybrids (direct release) against significantly sustained release in PN-R nanoconjugate (via polymeric media) through diffusion process. This is to mention that media permeation (water/PBS) has to occur first into the polymeric bulk when diffusion of drug can only be a feasible process in PN-R nanoconjugate and delayed diffusion or sustained release in PN-R is understood from the three step process; i) permeation of solvent molecules into the polymer matrix, ii) diffusion of drug molecules from intercalate to polymeric matrix, and iii) diffusion of

drug molecules from polymeric matrix to the release media. **Figure 4.6a** demonstrates the experimental evidence of considerably slow drug release from polymer matrix while very low permeation of water molecule in PCL matrix is well known [Messersmith et al., 1995]. Therefore, the (i) and (iii) processes are quite slow and are responsible for the sustained release of drug molecules from the PN-R nanoconjugate against the only (ii) process is operative in ZN-R or other drug intercalated LDHs make them fast release systems. The release rate of the drug molecules from the nanohybrids is mainly influenced by the factors like drug-host interactions, nature of the anions present in the interlayer gallery and the anions present in the PBS medium and LDH host layer and will be discussed in details in the next section. However, it is evident that the release of drug molecules from the PN–R nanoconjugate is more sustained and prolonged as compared to only drug intercalated LDHs systems.

A number of kinetic models such as Zero-order, first-order, Higuchi, Korsmeyer–Peppas, and modified-Freundlich kinetic models have been exploited to understand the release mechanism of drug molecules from the drug loaded nonohybrids [Dash et al., 2010; Mahanta et al., 2015]. The linear correlation coefficient (r^2) and other fitting parameter values obtained from the linear fittings of the drug release data with various mathematical models are given in **Table 2**. Among the used models, zero-order, first-order and Higuchi models give poor r^2 values ranging from 0.679 to 0.912 and are found not suitable to explain release mechanism while it was found that modified-Freundlich and Korsmeyer–Peppas models are most satisfactory for describing the mechanism of RH release from LDH-drug and PCL-(LDH-drug) matrix respectively (**Figure 4.6b**). The modified Freundlich model describes heterogeneous diffusion from the flat surfaces via both ion exchange and diffusion controlled phenomena. ZN–R, ZC–R and ZP–R system

are best fitted with modified Freundlich model with high linear correlation coefficients (r^2 ~ 0.98–0.99). For the PCL-RH and PN–R systems, Korsmeyer–Peppas model explain

Table 4.1: Rate constants, linear correlation coefficients (r^2) and diffusion release exponent (n) obtained by fitting the RH release data from ZN–R, ZC–R, ZP–R, PCL–RH and PN–R.

Sample	Zero-order		First-order		modified Freundlich		Higuchi		Korsmeyer-Peppas	
	k_0	r^2	k_1	r^2	k_M	r^2	k_H	r^2	n	r^2
ZN–R	54.5±3	0.889	1.71±0.34	0.816	0.42±0.23	0.975	78.3±3	0.912	0.68±0.13	0.941
ZC–R	68.1±2	0.944	2.46±0.42	0.917	0.37±0.11	0.973	88.6±2	0.921	0.802±0.18	0.928
ZP–R	79.8±4	0.946	1.79±0.33	0.912	0.14±0.06	0.956	111±6	0.917	0.309±0.08	0.899
PCL–RH	13.5±1.1	0.638	0.81±0.13	0.712	0.92±0.43	0.965	12.3±1	0.892	0.47±0.12	0.992
PN–R	0.68±0.14	0.679	0.01±0.14	0.626	1.06±0.23	0.961	7.37±0.5	0.945	0.51±0.17	0.991

the release phenomena more reasonably ($r^2 = 0.992$ and 0.991) leading to the exponent 'n' value of 0.47 and 0.51 respcetively, indicating the non-Fickian nature ($n \geq 0.45$) of drug release from the hybrid following the transport case-II. The delayed diffusion of the RH molecules from PCL–RH hybrid is assumed to be the presence of crystalline fringes present in the PCL matrix, which create a maze, called a 'tortuous path'. In PN–R the RH molecules release in a more sustained manner presumably due to the reason that they must first getting out from the LDH host layer and then they have to diffuse through the polymer matrix. **Figure 4.6c** schematically demonstrates the path through which the drug molecules released only from the LDH host layer and from the polymer-(LDH-drug) matrix. The cause of differential rate of drug release will be discussed thoroughly in the next section by using various analytical techniques such as XPS, UV-vis spectroscopy, DSC measurements, FTIR study etc.

4.2.4 Nature of interaction between the guest and host molecules: understanding of controlled release

The nature of interactions between the drug and host molecules is crucial to understand the differential controlled release behavior of the drug molecules from various drug nanohybrids. **Figure 4.7a** shows the XPS spectrum of Fe 2p appearing from LDH host layers before and after drug intercalation. In the XPS spectrum of all the three types pristine LDHs and their drug intercalated counterparts exhibit two signals at 711-715 eV and 725-727 eV corresponding to Fe $2p_{3/2}$ and Fe $2p_{1/2}$ respectively along with a satellite peak appeared at around 719 eV, are attributed to Fe^{3+} states coming from LDH host layer [Yamashita et al., 2008]. In all the cases it was found that the binding energies (BE) of both Fe $2p_{3/2}$ and Fe $2p_{1/2}$ states were shifted to higher binding energy side in drug intercalated LDHs as compared to pristine LDHs. The binding energies of Fe $2p_{3/2}$ obtained from ZN and ZN–R are 711.18 and 711.71 eV respectively; i.e., ΔBE= 0.53 eV and that of Fe $2p_{1/2}$ are 725.16 and 725.76 eV respectively; ΔBE= 0.60 eV. In case of ZC and ZC–R, the Fe $2p_{3/2}$ signal appeared at 711.72 and 711.93 eV respectively; i.e., ΔBE= 0.21 eV and the Fe $2p_{1/2}$ signals appeared at 725.33 and 725.57 eV respectively; ΔBE= 0.24 eV respectively. Again for ZP and ZP–R, Fe $2p_{3/2}$ peaks appeared at 712.51 and 712.57 eV respectively; i.e., ΔBE= 0.06 eV and the Fe $2p_{1/2}$ peaks appeared at 725.78 and 726.02 eV respectively; ΔBE= 0.24 eV respectively. Hence shifting of BE of Fe 2p peaks after drug intercalation is the highest for ZN system against the least increment in ZP system whereas moderate increment was observed for ZC system. The highest shifting of BE from ZN and ZN–R may be attributed from highest drug – LDH host layer interaction whereas smallest shifting was observed from ZP and ZP–R due to least drug – LDH host layer interaction. Similar results are also observed for Zn 2p peaks and the differences in binding energies of Zn $2p_{3/2}$ peaks are 0.03, 0.1 and 0.52 eV for ZP–R, ZC–R and ZN–R systems, respectively, as compared to their respective pure LDHs.

Again the difference in binding energies of Zn $2p_{1/2}$ peaks are 0.05, 0.22 and 0.54 eV for ZP–R, ZC–R and ZN–R systems, respectively, as compared to their respective pure LDHs. Hence, XPS investigation clearly indicates that drug molecules strongly interact with ZN while the extent of interactions goes down in ZC and ZP gradually.

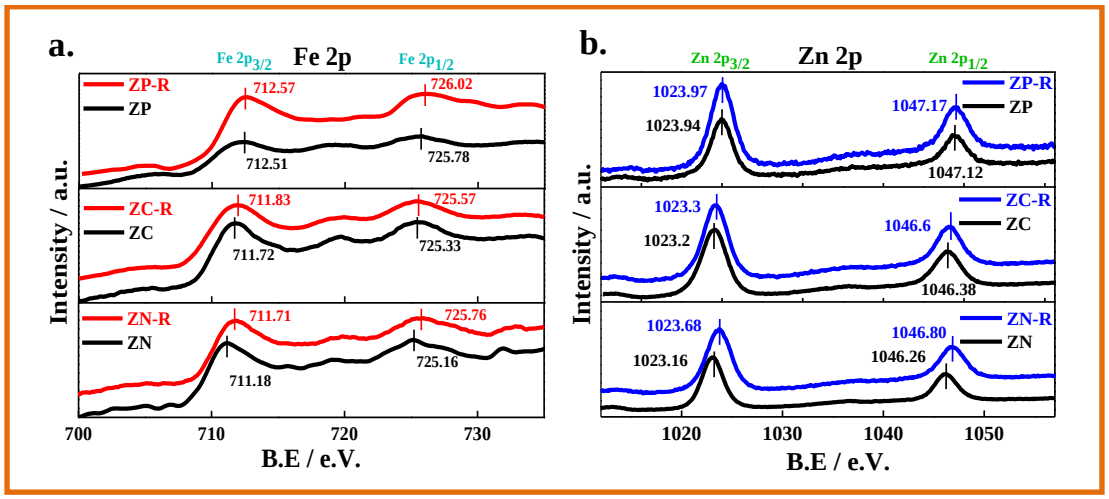

Figure 4.7: (a) Fe 2p and (b) Zn 2p XPS spectra for pristine LDHs and drug intercalated LDHs. The vertical lines indicate the peak position/binding energy.

The comparative solid state, diffuse reflection UV–Vis spectra of pristine LDHs, pure drug, drug intercalated LDHs and polymer nanocomposite are shown in **Figure 5c**. The

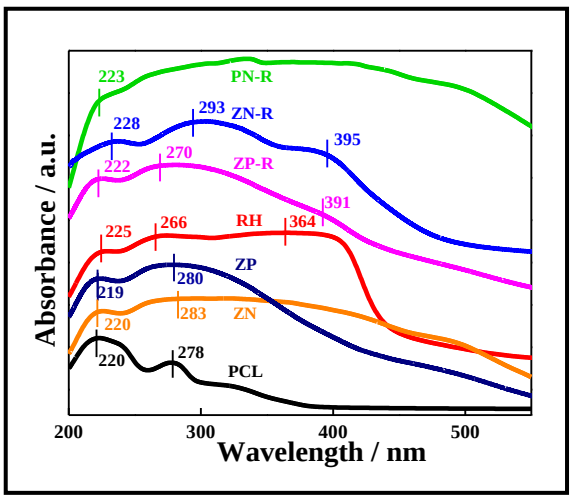

Figure 4.8: Comparison of solid-state UV−vis spectra of pristine LDHs (ZN), pure drug (RH), drug intercalated LDHs (ZN–R) and polymer nanohybrid (PN–R).

absorption spectrum of pure RH exhibits peaks at 225, 266 and 364 nm. The spectrum of pristine ZN shows strong UV absorption at 220 and 283 nm due to the presence of nitrate anions present in the interlayer galleries [Wang et al., 2015]. After intercalation, ZN–R exhibits absorption peaks at 228, 293 and 395 nm, with some prominent red shifting, which is due the interaction between the drug molecules and LDH host layers. Similarly, after intercalation, ZP–R also exhibits absorption peaks at 222, 270 and 391 nm, with some meager red shifting, which is due the lower interaction between the drug molecules and LDH host layers. After polymer nanocomposite formation, PN–R exhibits UV-vis absorption ability below 400 nm.

Differential scanning calorimetry (DSC) was further used to understand the interaction of between drug molecules and different types of LDH host layers before and after the introduction of polymer both qualitatively and quantitatively. DSC results, as shown in **Figure 4.9**, show a well defined endothermic peak (melting temperature, T_m) at 264 °C of pure drug, indicating its crystalline nature. The melting temperature of the intercalated drug in ZN-R has lowered by 41 ^oC to 223 °C from the melting point of pure drug at 264 °C (**Figure 4.9a**) while this temperature decrease becomes 13 ^oC only (264 → 251 °C) in ZP-R **(Figure 4.9c)** indicating greater interaction in ZN-R system as compared to ZP-R. Moreover, the heat of fusion of ZN-R has reduced significantly to 68 $J.g^{-1}$ from the pure drug of 85 $J.g^{-1}$ also supports the greater reduction in ZN-R vis-à-vis ZP-R (73 $J.g^{-1}$) due to better interaction in ZN-R. This is to mention that the melting of pure PCL is affected by the presence of ZN-R and increases the melting point of PCL to 64.4 ^oC from the pure PCL melting of 59 ^oC with significant peak broadening (**Figure 4.9d**). However, the effect of drug melting is not clear as the PN-R degrade before the melting temperature of drug.

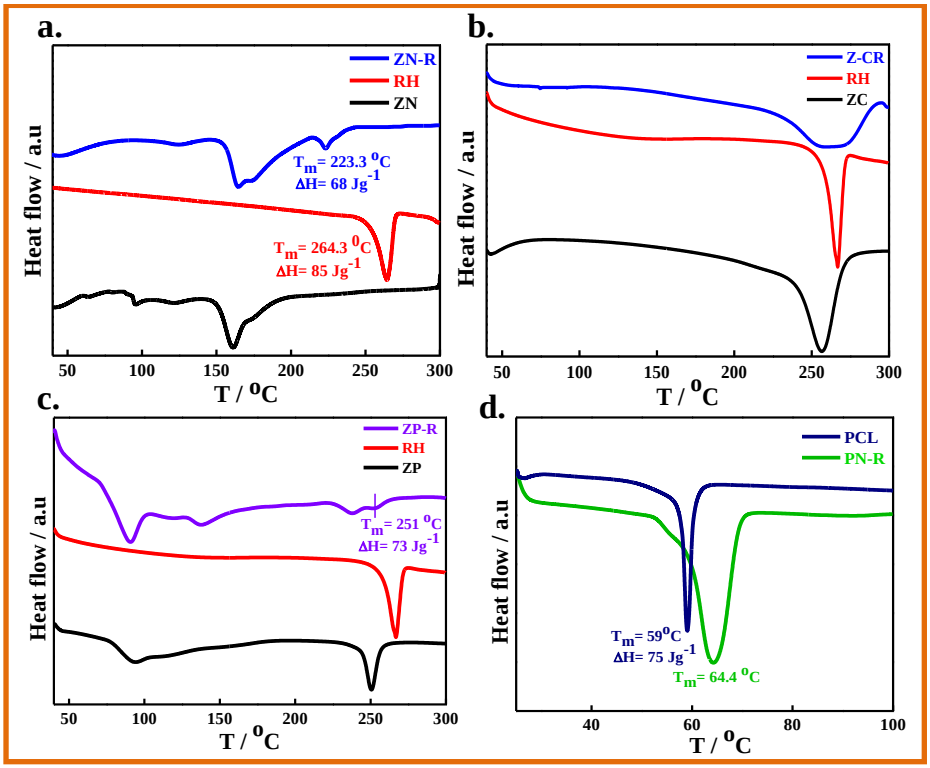

Figure 4.9: DSC thermograms of free drugs and drug intercalated LDHs, (a) nitrate LDH systems, (b) carbonate LDH systems, (c) phosphate LDH systems, and (d) pure polymer and polymer nanoconjugate.

Thermogravimetric analysis (TGA) was carried out to monitor the weight loss behavior of the samples under nitrogen atmosphere. Pristine PCL showed a simple one-step decomposition profile, as demonstrated by **Figure 4.10**. PCL started degrading at around

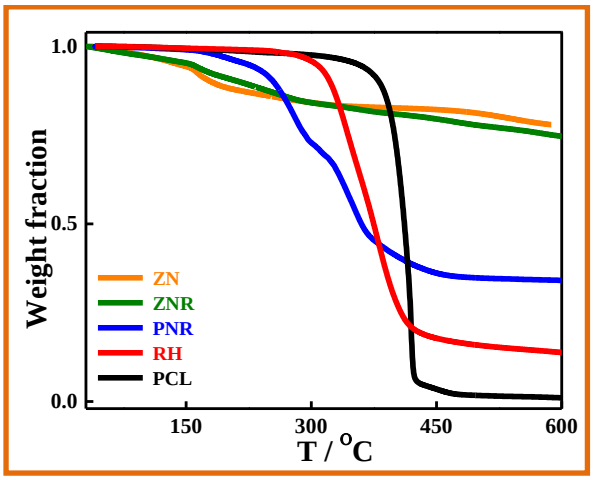

Figure 4.10: TGA thermograms of ZN, ZN–R, pristine PCL, pure drug and for PN–R systems.

310 °C and completely decomposition occurred at around 480°C. Three stages of weight loss behaviors are commonly observed in pristine LDHs. In the present study for ZN LDH, the weight loss steps occurred at 80–155 °C, 155–380 °C and 380–560 °C with ~ 5%, ~ 14% and ~ 6% weight loss respectively. The first stage of weight loss is associated with the loss of adsorbed water molecules along with hydrogen bonded water within the LDH layers, whereas the second weight loss step is associated with the dehydroxylation of LDH host layers and final weight loss resulting from the elimination of interlayer NO_3^- ions. The TGA curve of pure drug follows single stage degradation in the temperature range of 280–450 °C. Drug intercalated LDHs exhibits sour stage weight loss behaviors. Pristine PCL and LDH shows 5% weight loss 355 °C and 141°C. 5% weight loss occurs at 191 °C in ZN–R whereas 5% weight loss occurs at 223 °C in PN–R indicating higher thermal stability of the LDH after polymer wrapping.

The FTIR spectra pristine PCL, LDH, RH molecules, ZN–R hybrids and PN–R nanocomposites are shown in **Figure 2c**. The spectra of pristine ZN shows a broad band at 3468 cm^{-1}, which is attributed to the stretching vibration of the O–H groups both in the brucite-like layers of LDH and from the interlayer water molecules. The band at (1630 cm^{-1} appears due to bending vibration of interlayer water molecules. The sharp band at 1382 cm^{-1} is assigned to $,v-3.$ stretching vibration of the NO_3^- groups in ZN. The absorption bands below 1000 cm^{-1} are due to M–O and M–O–H vibration modes of LDH layers and the patterns are very similar to previous literature [Parida et al., 2012]. Pristine PCL exhibits characteristic peaks for carbonyl group at 1728 cm^{-1} ($\nu_{(C=O)}$) and ether group at 1172 cm^{-1} ($\nu_{(C–O–C)}$), which agree well with the previous literature [Rai et al., 2016]. The spectrum of pure raloxifene hydrochloride shows characteristic peaks at 3455(O–H stretching), 1643 cm^{-1} (C=O stretching), 1597cm^{-1} (–C–O–C– stretching), 1466 cm^{-1} (–S– benzothiophene), 1260 cm^{-1} (alkyl–O–phenyl stretching) and 905 cm^{-1}

(benzene ring). Presence of prominent drug peaks (at 1595 cm^{-1} and 1260 cm^{-1}) and dilution (low intense) of nitrate group peak at 1384 cm^{-1} confirming the replacement of nitrates ions with the raloxifene ions in the spectrum of ZN–R. The O–H stretching vibration band originating from both structural hydroxyl and interlayer water molecules of the brucite-like layers in pristine ZN appears at 3468 cm^{-1}, which is shifted to 3435 cm^{-1} in ZN–R due to interaction between the anionic drug molecules and LDH metal hydroxide layers. All the characteristic peaks of PCL (1728 and 1172 cm^{-1}) and ZN–R (at 1595 cm^{-1} and 1260 cm^{-1}) are also present in PN–R. However, the O–H stretching vibration of both structural hydroxyl and interlayer water molecules of the Brucite-like layers of LDH shifted to 3430 cm^{-1}. The spectrum of pristine ZC showed an intense band at around 1368 cm^{-1} associated with the carbonate ion and at 1640 cm^{-1} bending

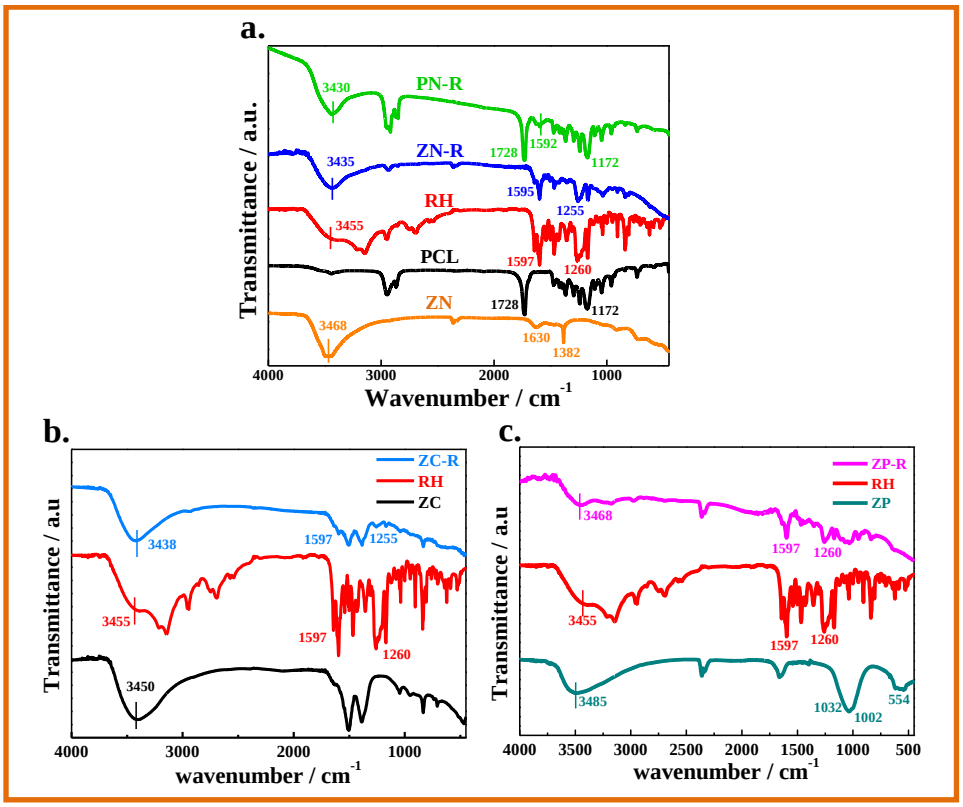

Figure 4.11: FTIR spectra of pristine LDH, pure drug and drug intercalated LDHs for (a) ZN systems, (b) ZC systems and (c) ZP systems.

vibration of interlayer water (**Figure 4.11b**). Similarly, ZP shows the characteristic peaks at 1098 cm^{-1} (asymmetric P–O str.), 1035 cm^{-1} (symmetric P–O str.), 965 cm^{-1} (asymmetric P–OH str.), and 535 cm^{-1} (asymmetric O–P–O str.) (**Figure 4.11c**). Drug intercalated carbonate and phosphate LDHs (ZC–R and ZP–R) show a broad absorption spectrum ranging from 3000 to 3600 cm^{-1} of both samples originates from the stretching vibration of O–H groups in the metal hydroxide sheets and from the interlayer water molecules. Again, the dilution of carbonate and phosphate group peaks and appearance of the drug peaks confirm the intercalation of raloxifene ions inside layers.

4.2.5 *In vitro* cytotoxicity

To evaluate the performance of raloxifene loaded developed materials, the relative anti-cancer efficiencies of pure drug (RH), RH intercalated LDHs, PCL–RH and PN–R were compared by assessing cell viability through MTT assay against HeLa cell line in a time and concentration dependent manner. Cells were incubated for 24 h, 48 h and 72 h with three concentrations of raloxifene (*i.e*. 10, 30 and 60 μg/ml) and with equivalent amount of drug loaded LDHs or with PCL composites. The above mentioned concentrations were chosen randomly to undertake the trial experiment for estimation of efficacy of the drug loaded developed materials compared to the pure drugs. It is well known that the biocompatibility of the vehicle is most important for biomedical applications. The biocompatibility of pure LDHs and pure PCL has been tested with growing number of cells as a function of concentration and time implying good biocompatibility of the LDH nanoparticles (**Figure 4.12**). Again, from **Figure 4.13a**, it can be seen that free raloxifene (RH), RH intercalated LDHs and PCL composites exhibited time dependent *in vitro* cancer suppression. RH delivery mediated by LDHs nanoparticles and PCL composites substantially enhanced cytotoxicity to HeLa cells compared to the free drug. As it shown

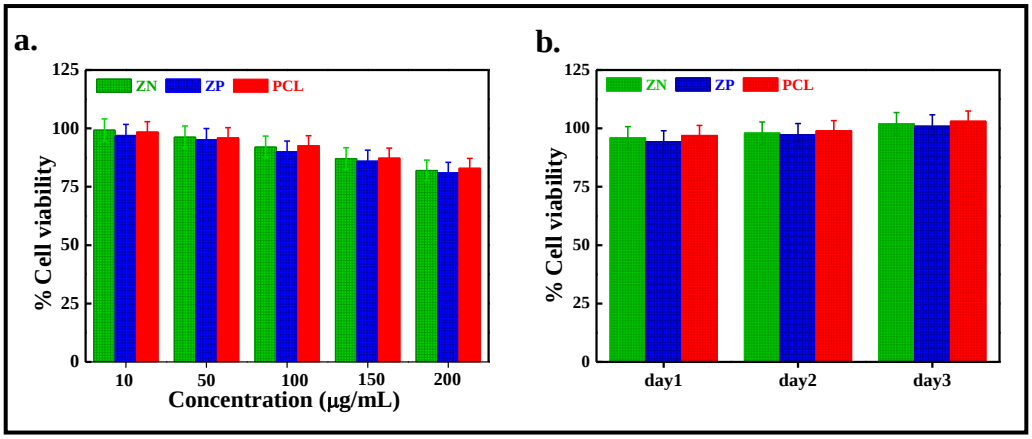

Figure 4.12: Percentage cell viability measured through MTT assay of HeLa cells after incubation of pristine LDHs (ZN, ZC and ZP) and pristine PCL with (a) different concentration range, and (b) different time frame.

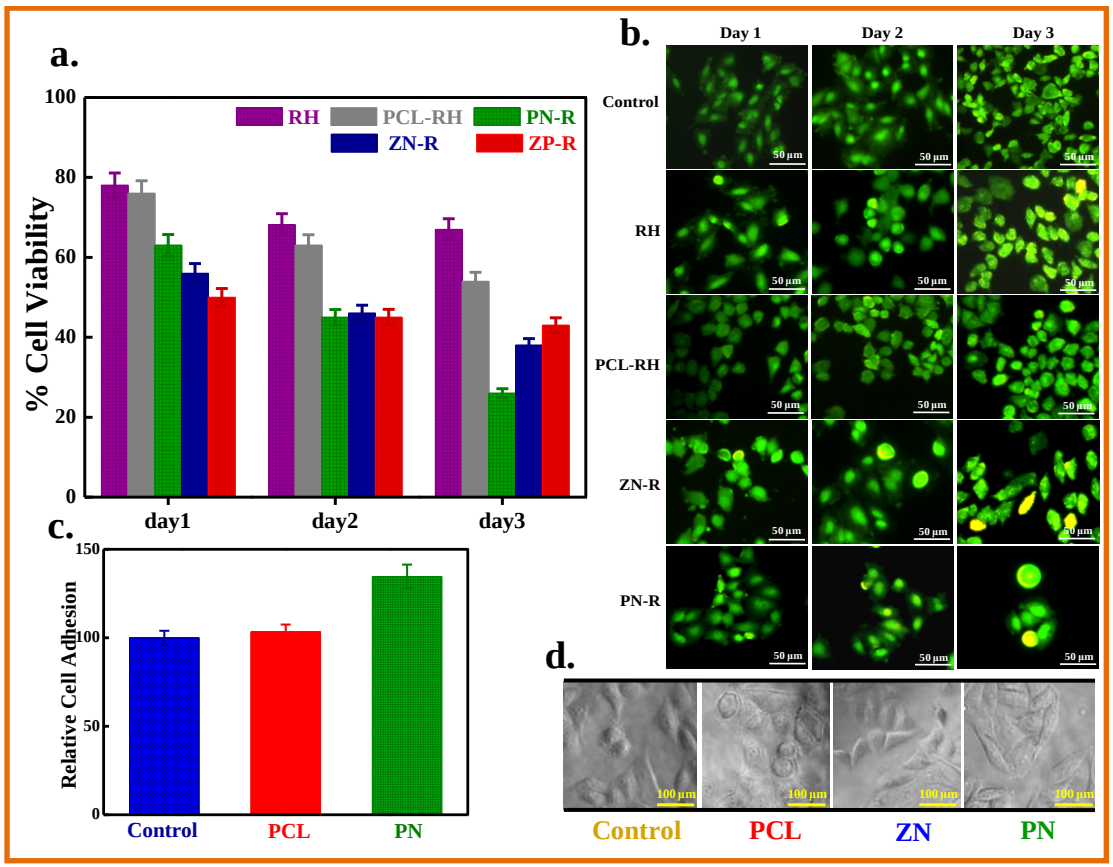

Figure 4.13: Comparative cell viability study of pure raloxifene, ZN-R, ZP-R, PCL-RH and PN-R against HeLa cells using MTT assay. (b) Fluorescent microscopic images of AO/ EtBr staining of the samples treated cells. (c) Relative cell adhesion values of the developed materials after 12 h incubation; (d) Phase contrast images of the HeLa cells grown on top of the indicated substrates after 12 h incubation.

in **Figure 4.13a**, for the HeLa cells incubated with 30 μg/ml free RH or with equivalent amount drug loaded developed materials, the cell viability (the survival rate) after 48 h post treatment was measured to be 43 ± 1.6%, 46 ± 1.7%, 48 ± 1.2%, 65 ± 2.4%, and 76± 2.1% for PN–R, LN–R, LP–R, PCL–R, and RH respectively. More interestingly, after 72 h treatment the cell viability decreased to 26 ± 1.8%, 38 ± 2.1%, 43 ± 3.1%, 58 ± 1.5%, and 71± 2.1% respectively. These results clearly demonstrated that PN–R exhibited the highest *in vitro* anti-cancer efficiency in comparison to the free drug. The highly dependence of cell viability (or cell mortality) of the developed drug conjugated materials on incubation time proves the of controlled and sustained drug release efficacy of the materials. The major interesting observation in this study was that although PCL-RH released the drug in a more sustained manner than the drug intercalated LDHs, however its cancer suppression efficacy was lower compared to the drug intercalated LDHs and PN–R. This finding may be understood from the better bioavailability of the drug in drug intercalated LDHs and PN–R compared to PCL-RH or free drug which will be uncovered in details in the next section.

To elucidate the mechanism of cell death and to confirm the potential of nanoparticles in inducing apoptosis, cells were stained with acridine orange (AO) and ethidium bromide (EtBr) and examined using a fluorescent microscope. This double staining helps us to distinguish the normal cells from apoptotic cells based on the permeability of cell membrane. Being cell-permeable, AO binds with DNA exhibiting green fluorescence while EtBr is selectively taken up by apoptotic cells and stained the condensed nuclei with red fluorescence [Byczkowska et al., 2013]. AO/EtBr staining cells observed as yellow-orange colored cells are apoptotic and necrotic cells were observed as red color fluorescence due to their loss of membrane integrity while healthy live cells were observed as green color fluorescence. The *in vitro* antitumor activity of raloxifene loaded

materials was monitored against HeLa cells as a function of time (after 1, 2, and 3 days of incubation) at a concentration of 30 μg ml^{-1}. From **Figure 4.13b** it is clear that, with increasing incubation time, ZN−R and PN−R treated cells exhibited apoptosis appearing bright green region with yellowish nuclear fragmentations and cell density also reduced due to killing of cells. The control cells were maintained without any treatment procedures and hence appeared green in fluorescence and there number density increases with time. Interestingly, it was observed the cell number density of pure drug treated cells was higher with very few apoptotic cells indicating poor killing performance of pure drug and PCL-RH as compared to drug ZN−R and PN−R. Therefore, cell viability and cell morphology studies strongly suggest that PN−R has the best *in vitro* anticancer efficacy compared to the pure drug or PCL-RH at the same drug concentration and exposure time, which implies that for the same therapeutic effect, the drug needed for the PN−R could be much less than that for the PCL-RH and Raloxifene itself. Hence the development of the PN−R thus can enhance the therapeutic effect as well as to increase the maximum tolerance dose of Raloxifene.

4.2.6 Cell adhesion

The cell-adhesion properties at the surface of pure PCL film and PCL-LDH nanocomposite (PN) films were evaluated by qualitative observation of morphological features as well as cell viability measurements. In control (tissue culture polystyrene plate), the cells adhered and spread moderately to the surface. In case of pristine hydrophobic PCL film surfaces, the cells adhered and grew to some extent; some of them remained rounded shaped and failed to adhere completely to the surface (**Figure 4.13d**). The cell-biomaterial interaction on the hydrophobic PCL surface is not the best. In contrast, for PN an enhanced cell adhesion and spreading was observed. The increase in cell adhesion of PN compared to pristine PCL may be attributed to the presence of

hydrophilic LDH molecules at the material surface (**Figure 4.13c**). The surface wettability of pure PCL and its LDH nanocomposite were determined through water contact angle measurement. The contact angle measurement showed that the water contact angle of PCL-LDH films (~ 67 ^{o}) decreased about 45^{o} compared to pristine PCL films (~ 112 ^{o}) while pristine LDH contact angle value was ~ 53^{o}. Thus an increment in hydrophilicity of PCL-LDH films facilitates cell adhesion and spreading on its surface. Again it is well known that cell adhesion property increased with surface roughness [Price et al., 2004]. From AFM height profile measurement it is obvious that PCL-LDH film has a very rough surface compared to pure PCL providing a better cell adhesive property.

4.2.7 Cellular uptake studies of rhodamine B labeled nanohybrids

The membrane permeability and internalization kinetics of LDH nanoparticles labeled with rhodamine B and LDH-polymer nanohybrids labeled with rhodamine B were investigated to validate its efficacy as a carrier to transport biomolecules into cells. For this study we have taken the concentration LDH–RdB as 100 μg ml^{-1} or equivalent amount of RdB for other materials as well. As shown in **Figure 4.14a**, ZP–RdB shows rapid initial uptake up to 6 h incubation, which then slows to a plateau. ZN–RdB exhibits rapid initial uptake up to 12 h incubation and the increases at slower rate. PN–RdB exhibits gradually uptake with 48 h of incubation. Cellular uptake of PN–RdB increased gradually with time due to the gradual internalization of ZN–RdB after getting released from PN–RdB nanohybrids. In contrast, rhodamine B and rhodamine B-labeled pristine PCL have very little uptake efficacy, which slowly increases with incubation time. From the above observations it can be concluded that free drug molecules cannot internalized into the cells easily due to repulsive interactions between the negative-charged cell membrane and negatively charged drug molecules, while the positively charged LDH

nanoparticles get attracted negatively charged cell membrane on its surface. However, the detailed mechanism of the LDH nanoparticles internalization into the cells is not yet well understood, it could proceed by the widely accepted endocytosis mechanism. Oh et al., demonstrated that the clathrin-mediated endocytosis is mainly responsible for the efficient internalization of LDH nanoparticles with an upper limit of 200 nm in size while the 350 nm LDH nanoparticles results a lower uptake through a non-selective internalization pathway [Oh et al., 2009]. Li *et al.* and Xu *et al.* also observed enhancement of cellular uptake of LDH nanoparticles in a concentration and time

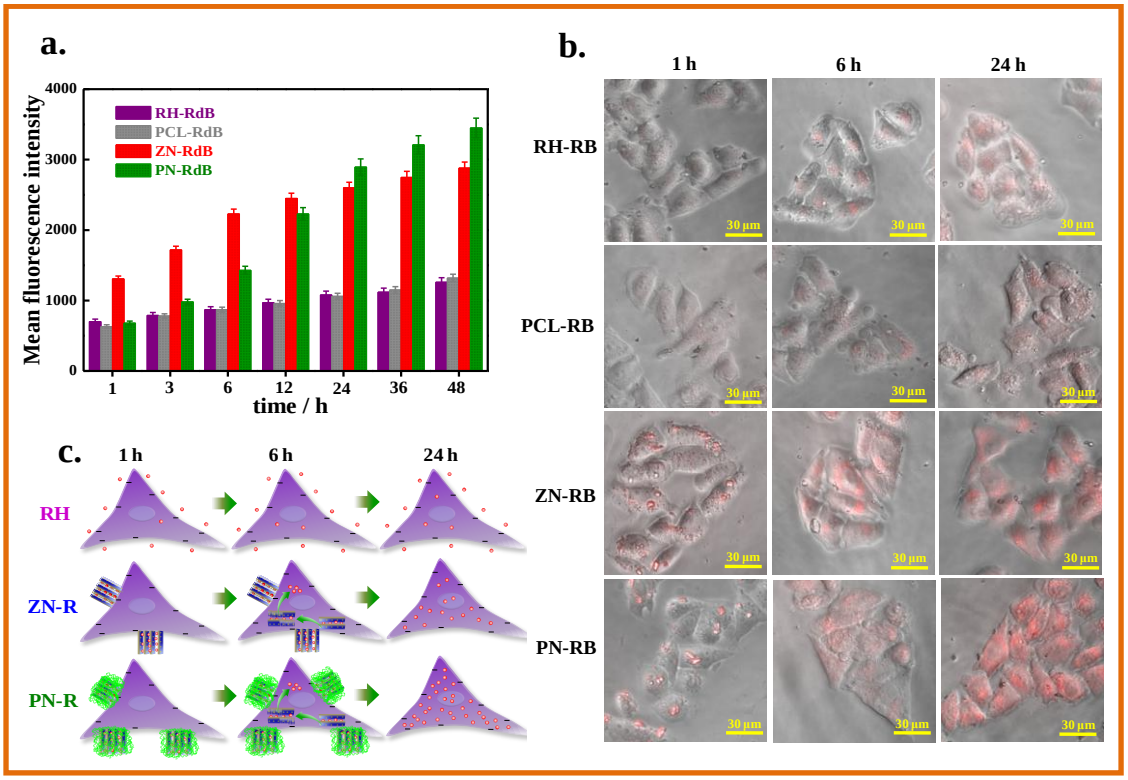

Figure 4.14: (a) Cellular uptake kinetics the developed materials into HeLa cells under different incubation times. (b) Fluorescence microscopic images showing the cellular uptake of rhodamine-B labeled samples into HeLa cells. Cells are exposed to 100 μg ml^{-1} or equivalent amount of RdB labeled particles showing various intensity of fluorescence depending on cellular uptake; and (c) Schematic illustration of cellular uptake mechanism considering same HeLa cell with indicated substrate with varying surface potential and roughness.

dependent manner [Li et al., 2013; Xu et al., 2008]. The significant enhancement of fluorescence intensity of PN nanocomposites over PCL may be understood from the fact that with incorporation of LDH in the PN nanocomposites enhances the cellular adhesion properties which facilitates better interaction between the cells and materials through docking.

Fluorescence microscopy observation (**Figure 4.14b**) also revealed that ZN–RdB and PN–RdB significantly enhanced the internalization of the nanoparticles compared to free drug or rhodamine–B labeled pure PCL. From **Figure 4.14b** it could be seen clearly that initially the positive charged rhodamine–B labeled LDH docks on the negatively charged cell membrane and can easily go into the cells through endocytosis. Whereas the negatively charged drug molecules make slow diffusion through the negatively charged cell membrane. After 2 h of incubation, all the rhodamine-B labeled samples were mainly accumulated in the cytoplasm showing red fluorescence. Although with increasing the incubation time to 24 h, all the samples show enhancement in fluorescence intensity. In rhodamine B and rhodamine-B labeled pure PCL the cytoplasm become brighter with increasing incubation time while the nuclei are staying dark as it was after 2 h of incubation, suggesting that most of rhodamine-B molecules transfected into cells did not enter the nuclei but stayed in the cytoplasm. In contrast, although initially (after 2 h of incubation) the nuclear fluorescence upon internalization of ZN–RB and PN–RdB) was weak, however after 24 h of incubation it becomes significantly bright red. Moreover the intensity of red fluoresce in PN–RdB is stronger compared to ZN–RdB. Previously, Xu *et al.* also showed that LDH-FITC nanorods mostly accumulated in the nucleus after 3 h of incubation [Xu et al., 2008]. **Figure 4.14c** schematically illustrates the mechanism of cellular uptake.

4.2.8 *In vivo* drug release study

The final goal of this study was to investigate whether these carriers can successfully deliver and control the RH concentration in blood plasma in an effective therapeutic range over a prolonged time period and to reduce the adverse side effects of anticancer drugs. To compare *in vivo* performance of free RH and the RH intercalated materials, the blood levels of RH concentration were measured after a single intravenous dosage of 10 mg kg^{-1} of free RH or equivalent amount in female Charles Foster albino rats. The mean plasma drug concentration versus time profile is plotted in **Figure 4.15**. The minimum

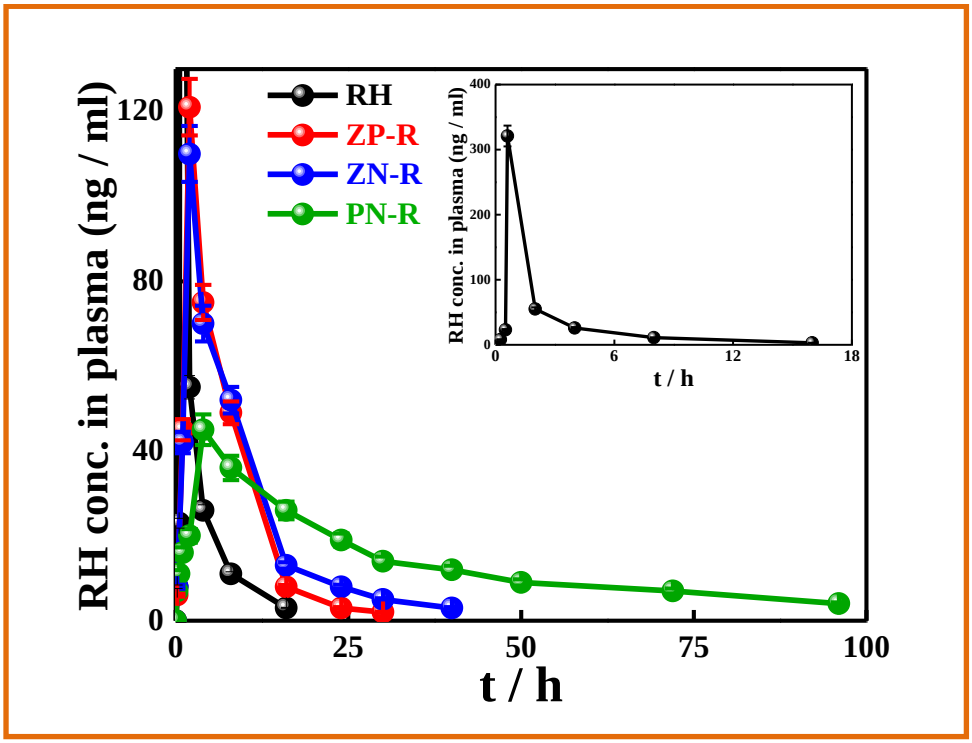

Figure 4.15: (a) Plasma drug concentration versus time profiles for RH, ZN-R, ZP-R and PN-R evaluated in Charles Foster albino female rats (n = 4) after intravenous administration at 10 mg drug / Kg body weight and equivalent amount in various delivery vehicles.

concentration of raloxifene needed to detect a significant decrease in cell number is 10^{-9} M (i.e., ~ 0.5 ng ml^{-1}) in human prostate cancer cell lines [Kim et al., 2002]. We chose a threshold of 1 ng ml^{-1} RH. The plasma concentration of free RH group showed a rapidly

declining profile with an initial burst release (C_{max} 321 ng / ml at 45 min) and complete release occurs within 10 h following administration. The plasma drug concentration for ZP–R and ZN–R systems show minimal initial burst release (C_{max} ~120 and 112 ng / ml respesctively) compared to free RH and moreover, their release sustained up to ~ 30 h and ~ 40 h for ZN–R and ZN–R system respectively. This extended release kinetics of ZP–R and ZN–R systems may be understood from the interaction between the intercalated negatively charged drug molecules and positively charged LDH layers. As ZN interacts more strongly with drug molecules compared to ZP, release of RH become more sustained for ZN–R system leading to slow clearance and correlates well with in vitro release data. After encapsulating the ZN–R into the PCL matrix (i.e. PN–R), the initial burst release was further suppressed, and more interestingly the duration of RH release was increased to 98 h.

4.2.9 Liver and kidney toxicity test: monitoring the effects of controlled drug release

Liver function tests (LFT) have been commonly used to examine hepatic dysfunctions. Activity of liver enzymes such as ALT and AST were studied to assess hepatotoxicity in the CF albino female rats after intravenous administration at 10 mg drug / Kg body weight and equivalent amount of samples. There was a significant increase in ALT (~115%) and AST (~175 %) activities in the rats that were treated with free RH compared to the control group after 1 day. However, as compared to pure RH treated group, PN–R treated group exhibits significant decrease in both ALT (~9%) and AST (~10%) activity. A meager increment of the liver enzymes activity (ALT and AST) was observed in ZN–R and ZP–R treated groups (**Figure 4.16**). Moreover, gradual abatement of liver enzymes activity with time was observed for all the treatment group rats. Serum urea and creatinine level were studied to further monitor the renal toxicity in all the treated groups. For first few days after treatment no significant increase in serum urea

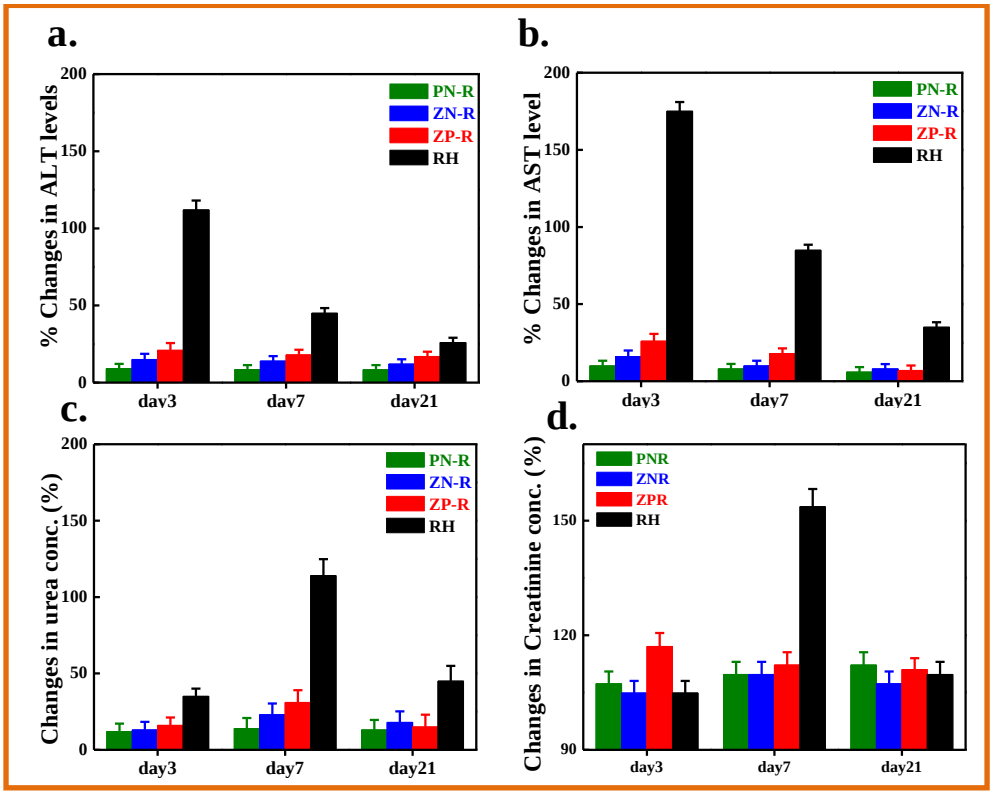

Figure 4.16: Changes of biochemical parameters as a function time: (a) alanine aminotransferase (ALT); (b) aspartate aminotransferase (AST); (v) urea and (d) creatinine activity at the 7th day in Charles Foster albino female rats after intravenous administration at 10 mg drug/Kg body weight and equivalent amount of drug intercalated materials. Results are expressed as mean ± SD, *n* =4.

and creatinine levels was observed **(Figure 4.16c,d)**. However, at day 7, rats treated with free RH exhibits significant elevation in serum urea and creatinine levels. The increase in serum urea and creatinine level was about ~114% and ~123%, respectively. As compared to free RH, all other treatment groups significantly brought down the elevated levels of serum urea and creatinine. Especially, in case PN–R treated group, the depression of levels of serum urea and creatinine was remarkably (~14% and ~11 % respectively). From the above discussion it is clear that the RH treated group experienced hepatic dysfunctions and renal toxicity where as in the PN–R treated group where the drug release in the most sustained manner has the highest protective ability against RH-induced damage of liver and kidney.

4.2.10 Histopathological findings

Histopathological evaluations are commonly used to investigate organ-specific effects of chemotherapeutic drugs. In the present study, hematoxylin and eosin (H & E) staining of the main organs including liver, kidney and spleen were used to evaluate the toxic effects pure drug and drug intercalated materials. As complied in **Figure 4.17**, analysis of liver tissues of rats in the control group shows normal architectural hepatocytes, which are large in size, hexagonal in shape with more or less centrally located one nuclei and homogenous cytoplasm. Similar results also observed for the PN–R treated group indicating no tissues were damaged. In contrast, hepatotoxic symptoms such as portal triad having bile ductular proliferation, deformation in shape and sizes of the hepatocytes and some inflammatory reactions also observed (indicated by blue arrows). Rats treated with ZN–R and ZP–R experienced no obvious hepatotoxicity. However, no significant histopathological abnormalities or lesions were observed in kidney and spleen in all the groups. It is worth mentioning that pristine LDHs have no toxic effects as illustrated by clinical chemistry and histopathology [Senapati et al., 2016;]

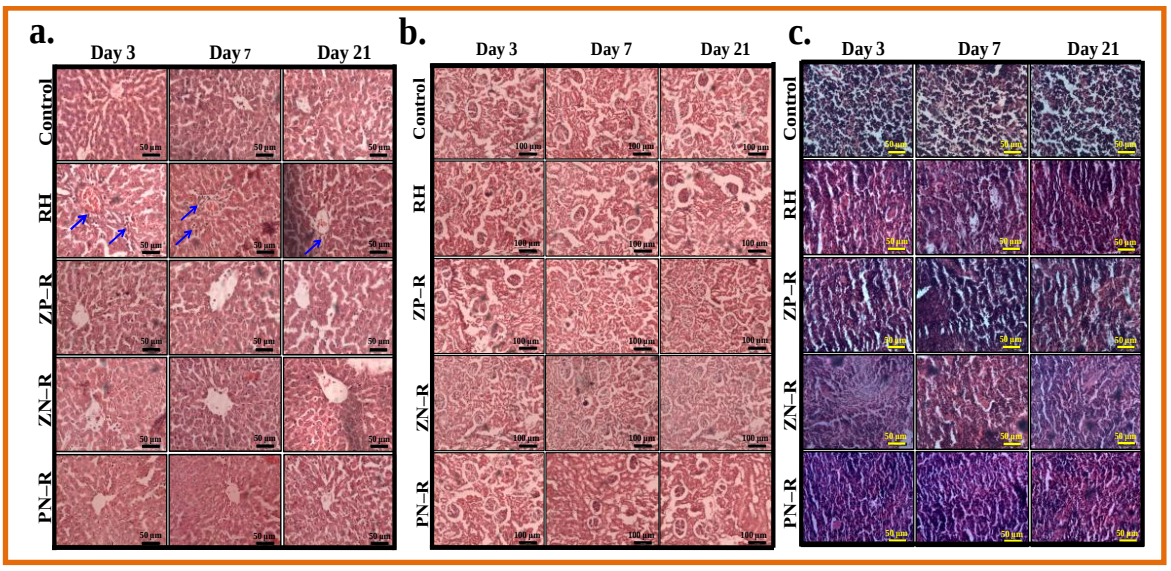

Figure 4.17: Histopathological examination using hematoxylin and eosin (H & E) staining to evaluate the toxicity of liver treated with control (PBS), pure RH, ZN-R, ZP-R and PN-R at different indicated time intervals.

4.3 Conclusion

A new anticancer drug delivery vehicle has been developed by intercalating the drug within the layers of two-dimensional layered double hydroxide nanocarrier followed by embedding them in a polymer matrix, called polymer nanohybrid. The level of drug intercalated LDH dispersion in polymer matrix is found to be uniform and surface charge (zeta potential) and roughness has been modified in presence of LDH in polymer matrix to make it suitable for cell biology. Considerable slow release of drug has been achieved in LDH with decreasing charge density of intercalant from PO_4^{-3} to CO_3^{-2} to NO_3^{-}. Polymer nanoconjugate (PN–R) demonstrates the best *in vitro* anticancer performance as compared to pure drug or drug embedded polymer (PCL-RH) as evident from *in vitro* cytotoxicity experiment. Better cell adhesion and cellular uptake efficiency has been obtained using polymer nanoconjugate. Sustained release of drug for prolonged time has been obtained *in vivo* system using albino rats as a function of time showing healthy lever and other body parts using polymer nanohybrid against damaged lever using free drug or drug intercalated LDH as revealed from the histopathological, lever and renal functional studies.